Distinct alpha-Synuclein species induced by seeding are selectively cleared by the Lysosome or the Proteasome in Neuronal Cells

Marina Pantazopoulou[1], Viviana Brembati[1*], Angeliki Kanellidi[1*], Luc Bousset[2], Ronald Melki[2], Leonidas Stefanis[1#]

[1]Biomedical Research Foundation of the Academy of Athens, Athens, 11527, Greece
[2]CEA and Laboratory of Neurodegenerative Diseases, Institut Francois Jacob (MIRCen), CNRS, 92265, Fontenay-Aux-Roses cedex, France
*These authors have equally contributed to this manuscript

[#]Correspondence to:
Dr Leonidas Stefanis
Biomedical Research Foundation of the Academy of Athens
4, Soranou tou Efesiou Street
Athens, Greece 11527
Email: lstefanis@bioacademy.gr
ORCID ID: https://orcid.org/0000-0003-3569-8990

Running title: Clearance of alpha-synuclein aggregates

Keywords: alpha-synuclein; lysosome; proteasome; aggregation; degradation; phosphorylation

Abbreviations used: α-Syn, alpha-synuclein; ALP, Autophagy-Lysosome Pathway; BAF, bafilomycin; CMA, chaperone-mediated autophagy; CNS, central nervous system; DLB, Dementia with Lewy Bodies; DOX, doxycyclin; EPOX, epoxomicin; GCI, glial cytoplasmic inclusions; HMW, high molecular weight; HRP, horseradish peroxidase; LB, lewy body; MSA, Multiple System Atrophy; PBS, phosphate-buffered saline; PD, Parkinson's disease; PFFs, pre-formed fibrils; PK, Proteinase K; PLK2, Polo-like kinase 2; pS129, phosphorylation at serine 129; PTM, post-translational modification; RAP, rapamycin; SDS, sodium dodecyl sulfate; UPS, Ubiquitin Proteasome System; WT, wild type.

Abstract

A major pathological feature of Parkinson's disease (PD) is the aberrant accumulation of misfolded assemblies of alpha-synuclein (α-Syn). Protein clearance appears as a regulator of the ''α-Syn burden" underlying PD pathogenesis. The picture emerging is that a combination of pathways with complementary roles, including the Proteasome System and the Autophagy-Lysosome Pathway, contributes to the intracellular degradation of α-Syn. The current study addresses the mechanisms governing the degradation of α-Syn species seeded by exogenous fibrils in neuronally differentiated SH-SY5Y neuroblastoma cells with inducible expression of α-Syn. Using human α-Syn recombinant fibrils (pre-formed fibrils, PFFs), seeding and aggregation of endogenous Proteinase K (PK)-resistant α-Syn species occurs within a time frame of 6 days, and is still prominent after 12 days of PFF addition. Clearance of α-Syn assemblies in this inducible model was enhanced after switching off α-Syn expression with doxycycline. Lysosomal inhibition led to accumulation of SDS-soluble α-Syn aggregates 6 days after PFF-addition or when switching off α-Syn expression. Additionally, the autophagic enhancer, rapamycin, induced the clearance of α-Syn aggregates 13 days post-PFF addition, indicating that autophagy is the major pathway for aggregated α-Syn clearance. Fibrillar phosphorylated α-Syn at S129 was only apparent at 7 days of incubation with a higher amount of PFFs. Proteasomal inhibition resulted in further accumulation of SDS-soluble phosphorylated α-Syn at S129, with limited PK resistance. Our data suggest that in this inducible model autophagy is mainly responsible for the degradation of fibrillar α-Syn, whereas the Proteasome System is responsible, at least in part, for the selective clearance of phosphorylated α-Syn oligomers.

1. Introduction

Genetic, neuropathological and biochemical data all point to a major role of the presynaptic protein alpha-synuclein (*α*-Syn) in the pathogenesis of Parkinson's Disease (PD) and related synucleinopathies, such as Dementia with Lewy Bodies (DLB) and Multiple System Atrophy (MSA) (Goedert et al., 2017). *α*-Syn, characterized by its structural plasticity, can adopt several conformational and oligomeric states; monomer with no defined structure, helical monomers and tetramers, *β*-sheet rich oligomer, protofibril and stable amyloid fibril (Melki, 2015, Uversky, 2003, Alam et al., 2019). OligomerizatIon and aggregation of *α*-Syn yields toxicity and neuronal dysfunction. *α*-Syn can self-propagate and spread among interconnected regions of the central nervous system (CNS) contributing to disease progression. In recent studies, the use of recombinant α-Syn pre-formed fibrils (PFFs) accelerates *α*-Syn toxicity and cell-to-cell transmission in both cell and animal models, pinpointing the prion-like properties of the protein (Luk et al., 2009, Volpicelli-Daley et al., 2011, Mougenot et al., 2012, Luk et al., 2012, Sacino et al., 2013, Masuda-Suzukake et al., 2013, Sacino et al., 2014c, Sacino et al., 2014b, Sacino et al., 2014a, Betemps et al., 2014, Bousset et al., 2013, Peelaerts et al., 2015). Moreover, post-translational modifications (PTMs), and in particular phosphorylation at serine 129 (pS129), are thought to be important for the transition between these pathological states, although the effect of phosphorylation is still controversial (Oueslati, 2016). There is however agreement that excess levels of *α*-Syn are pathogenic, presumably due to the dependence of aggregation on *α*-Syn concentration, which in turn affect neuronal homeostasis.

The mechanisms governing *α*-Syn degradation remain a subject of debate (Webb et al., 2003). The degradation of *α*-Syn, and its multiple oligomeric states, are thought to depend on two major intracellular protein degradation pathways; the Ubiquitin Proteasome System (UPS), and the autophagy-lysosome pathway (ALP) (macroautophagy, microautophagy and chaperone mediated autophagy-CMA) (Vekrellis et al., 2011, Stefanis et al., 2019). Impairment of either may result in accumulation of *α*-Syn leading to the development of PD and related synucleinopathies. Recently, it has been shown that pS129 *α*-Syn may act as a signal for its degradation, but the pathway involved (proteasome or macroautophagy) remains unclear (Waxman and Giasson, 2008, Chau et al., 2009, Machiya et al., 2010, Shahpasandzadeh et al., 2014, Arawaka et al., 2017). Although filamentous *α*-Syn can interact directly with the 20S proteasome and decrease its proteolytic activity (Lindersson et al., 2004), studies indicate that only a small fraction of soluble cell-derived oligomeric intermediates of *α*-Syn, and not monomeric, is degraded by the proteasome (Emmanouilidou et al., 2010). On the other hand, monomeric WT, but not mutant *α*-Syn is mainly degraded by the selective process of CMA; all forms can be cleared by macroautophagy (Webb et al., 2003, Cuervo et al., 2004, Vogiatzi et

al., 2008, Alvarez-Erviti et al., 2010). Additionally, overexpression of Polo-like kinase 2 (PLK2), the main kinase responsible for *α*-Syn phosphorylation in the brain, enhances *α*-Syn turnover *via* the autophagic degradation pathway (Oueslati et al., 2013, Dahmene et al., 2017). A similar observation has been reported in a yeast model of PD where the S129A mutation compromised the clearance of *α*-Syn *via* the autophagic degradation pathway (Tenreiro et al., 2014). Other cell culture studies have demonstrated that S129-phosphorylated *α*-Syn appears to be degraded by the UPS (Machiya et al., 2010, Arawaka et al., 2017), thus, contributing conflicting data concerning the pathways involved in *α*-Syn clearance. These apparent discrepancies arise as a consequence of different experimental systems, or of different pools of *α*-Syn analyzed (monomeric, oligomeric, fibrils), or even of different PTMs.

Of particular importance, given their transmission potential, are *α*-Syn species seeded by *α*-Syn fibrils. The manner of degradation of such seeded material has also been controversial. An earlier study suggested that this material, once formed, could not be cleared by intracellular protein degradation systems (Tanik et al., 2013), while more recent work provided support for the idea that the Autophagy Lysosome Pathway could degrade such material, once formed within cells (Gao et al., 2019). We have addressed this issue by using an inducible system that we have created for expression of untagged human *α*-Syn, and offers the advantage of being able to follow the clearance of *α*-Syn species following the shut-down of endogenous *α*-Syn expression with doxycycline (Vogiatzi et al., 2008, Vekrellis et al., 2009). Exposure of such cells to PFFs has enabled us to perform studies regarding the formation and clearance of seeded *α*-Syn species, and to dissect the pathways involved using pharmacological tools.

2. Materials and methods

2.1. Cell culture and treatment

SH-SY5Y cells were cultured in RPMI 1640 (R8758; Sigma-Aldrich), 10% fetal bovine serum (10,270; Gibco, Invitrogen, Carlsbad, CA, USA), and 1% penicillin-streptomycin (15140122; Thermo Fischer Scientific, Waltham, MA, USA). SH-SY5Y cells inducibly over-expressing WT human *α*-Syn were maintained in 200μg/mL G418 (345810; Merck KGaA, Darmstadt, Germany) and 50μg/mL Hygromycin B (10843555001; Merck KGaA, Darmstadt, Germany). *α*-Syn expression was switched off with doxycyclin (DOX) (1μg/ml) (D9891; Merck KGaA, Darmstadt, Germany). Stock cultures were maintained in the presence of DOX. Cells ($20.3x10^3/cm^2$) were plated on 10-cm culture dishes with 7ml of RPMI 1640. 10μM all-trans retinoic acid (554720; Merck KGaA, Darmstadt, Germany) was used to differentiate the cells. PFFs (Bousset et al., 2013), were added on the 4th day of differentiation at indicated amounts. Cells were washed with PBS 1d, 2d and 3d post-PFF for the experiment at

Fig. 1B, 2d post-PFF for Suppl. Fig. S1E, 4d post-PFF for Fig. 3B, and 5d post-PFF for the remainder. PFFs (5μg/μl) were stored at -80^{o}C and incubated for 3 min at 37^{0}C, before use. Epoxomicin (E3652; Merck KGaA, Darmstadt, Germany; 20nM) and Bafilomycin A1 (S1413; Selleck Chemicals; 100nM) were added for a 24h-incubation, and Rapamycin (BML-A275; Enzo Life Sciences, 1μM) for 48h.

2.2. Transmission Electron Microscopy (TEM)

Electron microscopy images were produced by adding 5 μl of PFFs on 200 mesh formvar-carbon film-bearing grids (Electron Microscopy Sciences, Hatfield, PA, USA), negatively stained with 2% w/w uranyl acetate (Sigma-Aldrich, USA) and examined in a Philips CM-10 TEM electron microscope (operating voltage: 60 kV).

2.3. Biochemical fractionation

Cells were harvested using Trypsin-EDTA (0.05%) (25200072; Thermo Fischer Scientific, Waltham, MA, USA), to digest extracellular cell-associated *α*-Syn fibrils, and lysed in STET buffer (150mM NaCl, 50mM Tris PH 7.6, 1% Triton X-100, 2mM EDTA; stored at 4°C), supplemented with protease inhibitors (11836153001; Sigma) and PhosSTOP Phosphatase Inhibitor (4906845001; Roche), followed by 30 min incubation at 4^{o}C. The lysates were centrifuged at 13.000xg for 30 min at 4^{0}C. The supernatant (Tx-soluble fraction) was collected and the protein concentration was estimated with the Bradford protein assay. The pellet (SDS-soluble fraction) was washed 2x with ice-cold PBS and resuspended in 2% SDS buffer (150mM NaCl, 50mM Tris pH 7.6, 2% SDS, 2mM EDTA; supplemented with Protease inhibitors (Sigma) and PhosSTOP Phosphatase Inhibitors (Roche)), probe sonicated and incubated for 15 min at room temperature (RT). SDS-containing sample buffer was added in the sequential fractions. The Tx-soluble fraction was incubated at 95^{o}C and the SDS-soluble fraction at 42^{o}C. 20μg of protein lysate (for the SDS-soluble protein loading we used the equivalent concentration measured in the Tx-soluble fraction) were resolved in 13% SDS-PAGE gel and transferred to nitrocellulose membranes, before blocking with 5% skim milk/TBST for 1h. Membranes were incubated in primary antibodies, overnight at 4°C and in HRP-conjugated secondary antibodies (Invitrogen) for 2h at room temperature. Primary antibodies used were rabbit monoclonal C20 (sc-6886; Santa Cruz Biotechnology, 1:1000); mouse monoclonal Syn-1 (610786; BD Biosciences, RRID:AB_398107; 1:1000); rabbit monoclonal pS129 *α*-Syn (ab51253; Abcam, RRID:AB_869973; 1:1000); mouse monoclonal tubulin gamma (T5326, Sigma-Aldrich, RRID:AB_532292; 1:5000); mouse monoclonal β-actin (12262; Cell Signaling Technology, RRID:AB_2566811; 1:5000); rabbit monoclonal c-jun (9165, Cell Signaling Technology, RRID:AB_2130165; 1:1000); rabbit polyclonal LC3 (PD014, MBL International, RRID:AB_843283; 1:2000); rabbit polyclonal p62 (PM045, MBL International, RRID:AB_1279301; 1:1000). The densitometry of immunoreactive bands was analyzed with ImageJ software.

2.4. Limited proteolysis

Cells were lysed in STET buffer, incubated for 30 min at 4°C and sedimented at 13.000xg for 30 min at 4°C. The supernatant (Tx-soluble fraction) was collected and the pellet was resuspended in ice-cold PBS and probe sonicated. Aliquots of each lysate (supernatant and PBS-dissolved pellet- 20 µl) were incubated with or without Proteinase K (P4032; Sigma-Aldrich, USA) for 10 min at 37°C at indicated concentrations, followed by SDS-containing sample buffer addition. Inactivation of Proteinase K and denaturation was performed at 95°C for the Tx-soluble fraction and at 65°C for the SDS-soluble fraction. Equal amounts of non-treated and PK-treated protein lysates, originating from the same protein sample, were analysed by SDS-PAGE.

2.5. Statistical analysis

GraphPad Prism 7 was used for the statistical analysis. Student's t-test was used when comparing two groups and one-way ANOVA with Bonferonni's correction for multiple groups. Statistical significance was set as * $p<0.05$, ** $p<0.01$, *** $p<0.001$ and data are presented as mean +/- SEM from 3, 4 or 5 independent cell culture preparations.

2.6. Immunocytochemistry

SH-SY5Y differentiated cells ($9.7x10^3/cm^2$), plated on poly-d-lysine-coated glass coverslips and cultured with 0.5 ml of RPMI 1640, were treated with PFFs at indicated amounts. The cells were washed with Trypsin-EDTA (0.0025%), prior to fixation with 3.7% formaldehyde. Blocking and permeabilization was performed with 5% normal goat serum (NGS)/0.2% triton-X100/PBS for 1h at room temperature. Cells were incubated with primary antibodies over night at 4°C and with secondary antibodies for 1h at room temperature. Primary antibodies used were mouse monoclonal Syn-1 (610786, BD Biosciences, RRID:AB_398107; 1:1000); rabbit monoclonal MJFR-14-6-4-2 (ab209538, Abcam, RRID:AB_2714215; 1/1000); mouse monoclonal 211 (sc-12767, Santa Cruz Biotechnology, RRID:AB_628318; 1/1000); mouse monoclonal D10 (sc-515879, Santa Cruz Biotechnology; 1/1000); mouse monoclonal SYN303 (824301, BioLegend, RRID:AB_2564879, 1/1000); rabbit monoclonal pS129 α-Syn (EP1536Y) (ab51253; Abcam, RRID:AB_869973; 1:1000), mouse monoclonal Tuj1 (MRB-435P-100, Covance, RRID:AB_663339; 1/1000). Fluorescent images were obtained at 40x and 63x objective magnification with a Leica SP5-II upright confocal microscope under constant settings of laser power, pinhole size, gain, and offset between the different conditions.

3. Results

3.1. Seeding and aggregation of endogenous α-Syn in SH-SY5Y differentiated cells upon PFF-addition

SH-SY5Y cells, with inducible expression of human *α*-Syn (under the control of Tet-off response element), were used to investigate the potency of exogenously applied recombinant *α*-syn PFFs (Suppl. Fig. S1A) to seed endogenous *α*-Syn into fibrillar aggregated species. Cells, constitutively overexpressing *α*-Syn (-DOX) or with suppressed expression of *α*-Syn (+DOX), were differentiated for 4 days and PFFs (0.5 μg) were added for one, two and three days (Fig. 1A). Western immunoblotting, using an antibody against total *α*-Syn (C20), of lysates from non-treated and PFF-treated cells, sequentially extracted with 1% Triton X-100, followed by 2% SDS, demonstrated that Tx-soluble *α*-Syn was nicely expressed in the –DOX and suppressed in the +DOX condition, while SDS-soluble *α*-Syn species were detected in both - and +DOX PFF-treated cells, but barely at all, at this exposure, in the absence of applied PFFs (Fig. 1B). Occasionally, and not consistently, faint HMW (high molecular weight) bands were detected in the lanes of Tx-soluble extracts of cells treated with PFFs (Suppl. Fig. S1B). Focusing on +DOX cells, in which *α*-Syn expression is downregulated with doxycycline, it is demonstrated that PFFs can be uptaken within 24 hours, a procedure that reaches a plateau after 48 hours of incubation. There was no difference in the amount of monomeric, truncated or oligomeric *α*-Syn between the + and the -DOX condition in the SDS-soluble material in these early time points, indicating that this material represented the introduced PFFs, rather than endogenous seeded *α*-Syn (Fig. 1B, D).

To overcome this time limitation, differentiated cells (- and +DOX) were incubated with different amounts of PFFs (0, 0.3, 0.5, 0.75, 1 and 1.5 μg) for six days. Upon fractionated immunoblotting, using the same antibody against total *α*-Syn (C20), it was demonstrated that six days after PFF-addition there was a clear increase in the amount of SDS-soluble monomeric, truncated and oligomeric *α*-Syn species in the -DOX compared to the +DOX cells, indicating that this represented seeding of endogenous *α*-Syn present within the -DOX cells into aggregated assemblies. In +DOX cells, there was limited detection of aggregated SDS-soluble *α*-Syn that probably corresponded to the internalized PFFs remaining in the cells, or to low level seeding of the low amounts of endogenous *α*-Syn present under these conditions (Fig. 1C, E; Suppl. Fig. S1C,D). In the Tx-soluble fraction, no alteration was detected in *α*-Syn levels, with or without PFFs. Using 0.2 μg of PFFs or less, in equivalent number of cells, no seeding was observed 6 days post-PFF addition (data not shown). PFF-dose titration indicated the minimal amount of PFFs (0.5-1 μg) with regards to maintaining a non-saturated cell system, permitting the comparison between - and +DOX cells, hence distinguishing endogenous seeded *α*-Syn from added recombinant PFFs. Comparing seeding of endogenous *α*-Syn, 2 and 6 days post-PFF addition, it is

demonstrated that SDS-soluble *α*-Syn species accumulated overtime in -DOX cells, however when *α*-Syn expression is suppressed (+DOX), internalized PFFs were cleared from the cells (Suppl. Fig. S1E), suggesting that endogenous *α*-Syn is indispensable for *α*-Syn highly aggregated species formation.

Proteinase K (PK) resistance is widely used to assess *α*-Syn aggregation propensity, indicative of the pathological properties of the protein (Mori et al., 2002, Neumann et al., 2004, Tanji et al., 2010, Pieri et al., 2016). To investigate PK-resistance of the SDS-soluble species, -DOX cells were incubated with PFFs for six days, lysed and fractionated. PK-treatment demonstrated that the SDS-soluble fraction is comprised to a large extent of aggregated PK-resistant *α*-Syn species; in the Tx-soluble fraction, *α*-Syn was degraded upon PK digestion (Fig. 1F).

Immunocytochemistry and confocal microscopy analyses were conducted in PFF-treated SH-SY5Y differentiated cells. Different amounts of PFFs (20, 50, 100 and 200 ng) were added in - and +DOX cells and incubated for six days. Staining with antibodies against total *α*-Syn (211) and aggregated *α*-Syn (MJFR-14) showed that *α*-Syn localized around the nucleus forming inclusions in -DOX cells (Suppl. Fig. S2A, B). In +DOX cells, residual *α*-Syn inclusions were detected, likely corresponding to the added PFFs or low-level seeding. 100ng of PFFs were used to further identify these inclusions with additional antibodies against total *α*-Syn (Syn1 and D10) and compare them with stainings against aggregated *α*-Syn (MJFR-14). In -DOX cells, endogenous *α*-Syn was localized to puncta as visualized by all three antibodies (Fig. 2A). In non-treated -DOX cells, stained with antibodies against total *α*-Syn (Syn1, D10), *α*-Syn is evenly distributed across the cytoplasm and processes, with a light punctate pattern of staining, whereas no signal was detected when stained with MJFR-14; in non-treated +DOX cells, no signal was observed (Fig.2A). Higher power magnification demonstrated perinuclear *α*-Syn inclusions depicting a clear difference between - and +DOX PFF-treated cells (Fig. 2B, Suppl. Fig. S2B). Double labelling immunofluorescent analysis of - and +DOX PFF-treated cells using D10, in conjunction with MJFR-14, confirmed the presence of endogenous *α*-Syn in the cytoplasmic inclusions (Fig. 2C). Co-staining with oxidized/nitrated *α*-Syn (SYN303) and MJFR-14 indicated the cytoplasmic distribution of *α*-Syn pathological aggregates; no staining with SYN303 was detected at baseline in the –DOX cells without PFFs (data not shown) or in +DOX cells with PFFs, indicating that the staining in the –DOX cells with PFFs represented endogenous seeded *α*-Syn with altered biochemical properties (Fig. 2D). Both biochemical and immunofluorescence data indicate that, in this inducible cell system, endogenous *α*-Syn is seeded six days after PFF-addition, forming pathological PK-resistant aggregates, localized around the nucleus.

3.2. Aggregation and clearance of endogenous α-Syn post-PFF treatment

To further elucidate the PFF-triggered endogenous *α*-Syn aggregation propensity and accumulation, we quantified endogenous *α*-Syn species over time (Fig. 3A). In -DOX

cells, 4, 6 and 12 days after PFF-addition, SDS-soluble α-Syn assemblies increased over time, reaching a plateau 6-12 days post-PFF addition. In +DOX cells, α-Syn aggregates corresponding to PFFs were cleared 12 days after PFF-addition (Fig. 3B, C). This inducible tet-off cell system allows the manipulation of α-Syn expression by adding doxycycline. Hence, exploiting this feature of our cell model, -DOX cells overexpressing α-Syn were treated with PFFs for 6 days and incubated with doxycycline for the following 6 days, in order to suppress α-Syn expression (6d-/6d+) (Fig. 3A). 6 days post-suppression, Tx- and SDS-soluble α-Syn levels were decreased, reaching α-Syn levels of +DOX cells (Fig. 3B, C), suggesting that endogenous α-Syn is indispensable for the formation of α-Syn aggregates and that, when shutdown, these species are targeted for degradation. Two, 4 and 6 days post-suppression (6d-/2d+, 6d-/4d+ and 6d-/6d+), α-Syn assemblies are gradually cleared from the cells. Likewise, PK-resistant species are gradually degraded (Fig. 3D, E). Lysing the cells with STET buffer resulted in partial PK-digestion due to the presence of Triton X-100, hence the incomplete digestion of γ-tubulin in the Tx-soluble fraction upon PK treatment. However, the presence of Triton X-100 did not seem to interfere with α-Syn PK-digestion. In the SDS-soluble fraction, the pellet was dissolved in PBS (detergent-free), followed by PK digestion and quenched with SDS-containing sample buffer. Non-treated and PK-treated samples originate from the same protein lysate, thus PK-treated bands were normalized to the γ-tubulin levels of the non-treated in the SDS-soluble fraction. Additionally, equal protein levels were further confirmed with ponceau staining (data not shown). Comparing the clearance rate of α-Syn aggregates post-suppression, in non-treated and PK-treated SDS fractions, it is demonstrated that SDS-soluble PK-resistant α-Syn is cleared at the same rate as the non-PK-treated (Fig. 3F). Altogether, these data introduce a novel cell system where fine-tuning α-Syn expression could prove a powerful tool for elucidating the pathways involved in aggregated α-Syn clearance, addressing exclusively degradation, instead of the equilibrium between aggregation and degradation rates.

3.3. Lysosomal inhibition leads to accumulation of PFF-induced α-Syn aggregates

To discern the pathways involved in the clearance of PFF-triggered endogenous α-Syn aggregates, we used pharmacological inhibitors that target either the lysosome (bafilomycin) or the proteasome (epoxomicin). To determine whether the lysosome is involved in the degradation of endogenous α-Syn aggregates, PFF-treated cells (-DOX, +DOX and 6d-/6d+) were incubated on day 5 and 11 with or without 100nM bafilomycin for 24 hours. At day 6 and 12, the accumulation of α-Syn assemblies was assessed after fractionation by western immunoblotting. Increased levels of HMW species of SDS-soluble α-Syn were associated with lysosomal inhibition at day 6 (Fig. 4A,C). Shutting down the expression of α-Syn by adding doxycycline (DOX) on day 6 post-PFF addition resulted in the clearance of α-Syn assemblies over a period of 6 days (6d-/6d+) and this clearance was partially reversed upon bafilomycin treatment,

suggesting that the lysosome is involved in the clearance of the seeded material (Fig. 4A,B). Analysis of p62 and LC3 levels, established markers of autophagosome/lysosome activities (Tanida et al., 2008), in non-treated and PFF-treated cells, demonstrated that bafilomycin had the desired effects of increasing p62 and LC3-II (Fig. 4A), while it also served to show that there was no discernible impairment of lysosomal function at early or late time points when treating the cells with this particular amount of PFFs (Suppl. Fig. S3A,B, Fig. 4A). Further data suggested that upon proteasomal inhibition with 20nM epoxomicin (Epox), no accumulation of SDS-soluble *α*-Syn was observed (Suppl. Fig. S3C). 12 days post-PFF, lysosomal inhibition with bafilomycin in -DOX and 6d-/6d+ cells led to accumulation of SDS-soluble PK-resistant *α*-Syn aggregates (Fig. 4D,E). Our data indicate that highly aggregated *α*-Syn species seeded by exogenous PFFs are targeted to the lysosome for degradation.

Immunocytochemistry and confocal microscopy analyses were conducted in PFF-treated cells to investigate the pathways implicated in aggregated *α*-Syn degradation. At day 5 and 11, cells (-DOX, +DOX and 6d-/6d+) were treated with bafilomycin or epoxomicin for 24 hours, followed by staining with the MGFR-14 antibody (Fig. 4F). In agreement with the biochemical analysis, fluorescence microscopy data demonstrated increased presence of aggregated *α*-Syn in the 6d-/6d+ condition only in the presence of bafilomycin, indicating that the lysosome is responsible for the selective clearance of *α*-Syn inclusions when *α*-Syn expression is down-regulated.

3.4. Autophagy is responsible, at least in part, for the clearance of fibrillar α-Syn

The autophagy–lysosomal pathway (ALP), involved in the degradation of long-lived proteins, is categorized into three groups: macroautophagy, chaperone-mediated autophagy and microautophagy. Rapamycin, which activates macro- and micro-autophagy through inhibition of the mTOR pathway, is widely used *in vitro* and *in vivo* to enhance clearance of autophagic substrates (Bove et al., 2011). For this purpose, rapamycin was used in order to investigate the degradation pathway of aggregated *α*-Syn. PFF-treated cells (-DOX, +DOX and 6d-/7d+) were incubated with rapamycin at day 5 and 11 for 48 hours (Fig. 5A). Fraction analysis with immunoblotting revealed that, 13 days post-PFF addition, SDS-soluble *α*-Syn is cleared in both d13 and 6d-/7d+ cells (Fig. 5B,C), indicating that autophagy (micro- or macro-) is responsible for the degradation of highly aggregated *α*-Syn species. At day 7, a trend for a decrease of *α*-Syn levels was observed upon rapamycin treatment, but did not reach statistical significance due to the variability across experiments. Tx-soluble *α*-Syn levels were not affected upon autophagic activation.

3.5. The Proteasome System is responsible for the selective clearance of PFF-induced phosphorylated α-Syn aggregates

Accumulating data suggest that *α*-Syn phosphorylation at S129 (pS129 α-Syn) is critical for *α*-Syn pathogenicity, suggesting a major role of pS129 *α*-Syn in the progression of Parkinson's disease (Gribaudo et al., 2019, Oueslati, 2016). Previous studies have already investigated the degradation pathway of soluble pS129 *α*-Syn, with contradictory results (Waxman and Giasson, 2008, Chau et al., 2009, Machiya et al., 2010, Shahpasandzadeh et al., 2014, Arawaka et al., 2017). To examine this issue in our cell system, differentiated cells were treated with epoxomicin or bafilomycin, and immunoblotting analysis with an antibody specific for pS129 α-Syn was undertaken (Fig. 6A,B). In epoxomicin-treated cells, pS129 *α*-Syn was increased 3.5-fold, whereas bafilomycin had no effect. Bafilomycin and epoxomicin co-treatment had no additive effect on pS129 *α*-Syn levels. These results indicate that the proteasome, and not the lysosome, is responsible for the degradation of pS129 α-Syn in this cellular system. To address the role of phosphorylation at S129 in *α*-Syn aggregation propensity, cells were treated with 0.75μg PFFs and fractionated immunoblotting with anti-pS129 was performed. No signal was detected in the SDS-soluble fraction after 6 days of PFF-incubation (data not shown). Incubating the cells with 0.5 and 1.5 μg of PFFs for 12 days, *α*-Syn aggregated species accumulated upon increased amount of PFFs, however pS129 *α*-Syn was barely detected (Suppl. Fig. S4A). Using high-dose PFFs (3μg), fractionated immunoblotting revealed that fibrillar pS129 *α*-Syn was only apparent relatively late, at 7 days post-PFF treatment (Fig. 6C), indicating that increased levels of *α*-Syn aggregates are required for the formation of SDS-soluble pS129 *α*-Syn species. Pharmacological inhibition of the proteasome led to further accumulation of pS129 *α*-Syn (Tx- and SDS- soluble) (Fig. 6C), indicating that the Proteasome System was, at least in part, involved in the selective clearance of these fibrillar phosphorylated forms of the protein. Using S129A PFFs, which cannot be themselves phosphorylated, we found that we could still produce pS129 *α*-Syn aggregated species, confirming that the pS129 *α*-Syn aggregates observed largely correspond to endogenous SDS-soluble *α*-Syn (Suppl. Fig. S4B). However, the detection of HMW pS129 *α*-Syn species in +DOX cells (Fig. 6C) does not exclude the possibility that PFFs themselves could be phosphorylated to a limited extent. Alternatively, such findings may indicate low-level seeding of endogenous *α*-Syn in the +Dox condition. Confirming our observations, S129-Phosphorylated *α*-Syn puncta were observed using fluorescence confocal microscopy only upon proteasomal inhibition with epoxomicin (Fig. 6D).

To investigate pS129 *α*-Syn aggregation and degradation over time, we examined SDS-soluble pS129 *α*-Syn 7 and 9 days post-PFF addition. The short half-life of pS129 *α*-Syn permitted the reduction of *α*-Syn shutdown period to two days (7d-/2d+). After 7 and 9 days of high-dose PFF treatment, differentiated cells (- or +DOX and 7d-/2d+), untreated or treated with epoxomicin for 24 hours (Fig. 6E), were subjected to

fractionated western immunoblotting (TX-100 and SDS fraction) with anti-pS129. Proteasomal inhibition led to accumulation of pS129 *α*-Syn (both Tx- and SDS-soluble) in d7 and 7d-/2d+ cells (Fig. 6F,G,H). After 9 days of PFF-treatment, pS129 *α*-Syn aggregates were highly decreased, and a consequent increase in the Tx-soluble fraction was observed, probably due to high dose PFF-induced cell toxicity. Upon bafilomycin treatment, no accumulation was observed (Suppl. Fig. S4C). 7 days post-PFF, PK- treatment of the cell lysates demonstrated that a small fraction of SDS-soluble pS129 *α*-Syn species is PK-resistant (Fig. 6I). Proteasomal inhibition did not lead to accumulation of pS129 *α*-Syn aggregates when treated with PK, suggesting that the species previously observed to accumulate with epoxomicin treatment correspond to oligomeric forms that are relatively more soluble, with decreased PK-resistance.

4. Discussion

Numerous studies have recently addressed the neuroprotective role of protein homeostasis in *α*-synucleinopathies (Manecka et al., 2017). It is especially important to understand the mechanisms underlying *α*-Syn aggregation and clearance, critical in the pathogenesis of Parkinson's Disease and related synucleinopathies. To obtain mechanistic insight into the degradation systems dictating the levels and conformers of *α*-Syn, we investigated the turnover of PFF-induced *α*-Syn assemblies in differentiated SH-SY5Y neuroblastoma cells, with inducible expression of human *α*-Syn. In line with a recent study (Gao et al., 2019), our data showed that PFFs induce the seeding of endogenous PK-resistant *α*-Syn species within a time frame of 6 days (Fig. 1,2). Studies on endocytosis and trafficking of recombinant *α*-Syn fibrils demonstrated that PFFs remain in the endolysosomal pathway following proteolysis through the lysosome (Sacino et al., 2017, Karpowicz et al., 2017) and a minority of the internalized material can escape the endocytic pathway to seed the recruitment of endogenous *α*-Syn into pathological assemblies (Karpowicz et al., 2017), in particular upon endocytic vesicle fusion with the lysosomal compartment (Flavin et al., 2017). Moreover, amyloid assemblies, including *α*-Syn PFFs, exhibit the ability to induce vesicle rupture, a process probably leading to the formation of proteinaceous inclusions such as Lewy bodies, due to the inability of cells to degrade ruptured vesicles and their content (Flavin et al., 2017). Our data indicate that at early time points, seeding of endogenous *α*-Syn was not observed, suggesting that PFFs probably remain in the endolysosomal compartment before becoming available for endogenous *α*-Syn seeding.

Aggregated *α*-Syn was still prominent 12 days post PFFs and shutting down the expression of *α*-Syn by adding doxycycline (DOX) on the 6th day after PFF-addition resulted in the clearance of *α*-Syn assemblies over a period of 6 days (6d-/6d+) (Fig.

3). This inducible cell model could prove a valuable tool for further elucidating the mechanisms underlying α-Syn assemblies degradation. Lysosomal inhibition with bafilomycin resulted in the accumulation of α-Syn aggregates both in d6 and 6d-/6d+ cells. 12 days post-PFF, bafilomycin treatment had no effect on the levels of α-Syn aggregates, however treatment with PK led to accumulation of SDS-soluble PK-resistant α-Syn species (Fig. 4). Activation of autophagy with rapamycin (macro- or micro-) induced the clearance of α-Syn assemblies 13 days post-PFF (Fig. 5), further implicating the Autophagy-Lysosome pathway (ALP) in this process. Evidence supports the role of α-Syn aggregates in the inhibition of autophagy (Winslow et al., 2010, Volpicelli-Daley et al., 2014, Mazzulli et al., 2016). However, in our cell model, when using low amounts of fibrils, lysosomal function does not seem to be impaired, as levels of LC3-II and p62 remained unaltered (Suppl. Fig. S3). Our data, together with others (Sacino et al., 2017, Gao et al., 2019), indicate that the lysosome is the most efficient pathway for degrading seeded α-Syn aggregates.

Although the role of phosphorylation of α-Syn at Ser129 in the pathophysiology and toxicity of the protein is controversial, pS129 α-Syn still consists one of the best indicators of pathological α-Syn inclusion formation (Fujiwara et al., 2002, Anderson et al., 2006, Waxman and Giasson, 2008, Waxman and Giasson, 2010, Karampetsou et al., 2017). Using low amount of PFFs, we were unable to detect SDS-soluble phosphorylated species. However, incubation with excess amount of fibrils induced the formation of insoluble pS129 α-Syn (Fig. 6, Suppl. Fig. S4). Our data indicate that recruitment and aggregation of endogenous α-Syn precedes the process of pathological pS129 α-Syn formation. Provided that modulation of pS129 α-Syn levels could affect α-Syn toxicity and disease progression in synucleinopathies, the degradation mechanism(s) involved could possibly represent a viable therapeutic target. Evidence suggests the involvement of the Proteasomal System in the degradation of soluble and insoluble pS129 α-Syn, with the lysosome playing a complementary role in the process (Machiya et al., 2010, Arawaka et al., 2017, Peng et al., 2018). In the current study, proteasomal inhibition with epoxomicin induced further accumulation of pS129 α-Syn (Tx- and SDS- soluble); however this increase of pS129 α-Syn aggregates corresponds to oligomeric forms with limited PK-resistance. Shutting down expression of α-Syn with doxycycline, resulted in the clearance of pS129 α-Syn aggregates, a phenomenon reversed upon epoxomicin inhibition. Our cell model proved to have some limitations regarding the investigation of pS129 α-Syn assemblies at later time points, since the use of excess fibrils resulted in increased toxicity 9 days post-PFF treatment. Lysosomal inhibition exhibited no effect on pS129 α-Syn levels (Tx- and SDS- soluble), however this result does not exclude the implication of ALP in the degradation of different conformers of the protein. Controversial studies suggest the implication of the lysosome in the degradation of phosphorylated at S129 α-Syn, however this can be associated to the differential conformational states of α-Syn, cellular stress or the crosstalk among

distinct post-translational modifications (Stefanis et al., 2019). Altogether, our data designate the essential role of the Proteasome System in the clearance of soluble and oligomeric pS129 *α*-Syn species.

Tanik et al. (Tanik et al., 2013) established a model of seeding, investigating *α*-Syn aggregation and degradation when excess amount of fibrils is used. This study addressed pS129 and total monomeric SDS-soluble *α*-Syn levels and reported that the aggregates formed persisted even after suppression of *α*-Syn gene expression for 72h, and that *α*-Syn levels remained unaffected when the lysosome is impaired. In our study longer suppression of *α*-Syn resulted in the clearance of the aggregates and the use of low amount of fibrils did not affect lysosomal activity. In line with Tanik et al. (Tanik et al., 2013), pS129 and total monomeric SDS-soluble *α*-Syn levels remained unaffected upon lysosomal impairment. Additional studies support the association of pS129 *α*-Syn fibrils with both autophagic components and the 20S Proteasome. Interestingly, pS129 *α*-Syn aggregates undergo incomplete autophagolysosomal degradation, generating highly neurotoxic *α*-Syn species that induce mitochondrial toxicity and mitophagy (Grassi et al., 2019). Accordingly, pS129 *α*-Syn aggregates seem to be resistant to lysosomal degradation suggesting, together with our data, the pivotal role of the Proteasome System in the clearance process. We do not view our results in contradiction to the findings of Tanik et al. (Tanik et al., 2013), as in our study Proteinase K resistant species of pS129 *α*-Syn did not change upon proteasomal inhibition, and are thus likely to resist degradation by proteolytic systems when very insoluble, as presumably occurred in their study.

Collectively, the current study demonstrates that autophagy (macro- or micro-) seems to serve as the major pathway for clearance of highly aggregated *α*-Syn assemblies whereas the Proteasome System is implicated in the degradation of phosphorylated at S129 *α*-Syn oligomers (Fig. 7). Our findings that different degradation pathways induce the clearance of distinct *α*-Syn aggregated species represent new and important insights into the biology of *α*-Syn aggregation and turnover. This well established cell model can prove an essential tool to assess aggregation and turnover of *α*-Syn assemblies as well as the role of different post-translational modifications (i.e. phosphorylation, ubiquitylation, truncation, sumoylation) and their effect on oligomerization, and to further screen for modifiers affecting *α*-Syn aggregation, clearance, secretion and cell-to-cell transmission. A deeper understanding of the mechanisms underlying aggregation propensity and clearance may help design novel strategies for regulating the levels of toxic *α*-Syn conformers and eventually develop a treatment for PD and related synucleinopathies.

Acknowledgements

We are grateful to Dr. Mantia Karampetsou for sharing her expertise on cell culture and PFF manipulation. We thank Dr. Stamatis Pagakis, Bioimaging Core Unit of BRFAA, for technical assistance and Ismini Kloukina for assistance with acquisition of EM images. This project has received funding from the Innovative Medicines Initiative 2 Joint Undertaking under grant agreement No 116060 (IMPRiND). This Joint Undertaking receives support from the European Union's Horizon 2020 research and innovation programme and EFPIA. This work is supported by the Swiss State Secretariat for Education, Research and Innovation (SERI) under contract number 17.00038. The opinions expressed and arguments employed herein do not necessarily reflect the official views of these funding bodies.

Competing interests

The authors declare that they have no competing interests.

Author contributions

MP conceived, performed and analyzed experiments, prepared figures and co-wrote the manuscript; VB and AK performed experiments; RM supervised and LB produced and characterized α-Syn assemblies; and LS conceived, analyzed experiments, and co-wrote the manuscript. MP, LB, RM and LS contributed to editing and finalizing the manuscript.

References

ALAM, P., BOUSSET, L., MELKI, R. & OTZEN, D. E. 2019. alpha-synuclein oligomers and fibrils: a spectrum of species, a spectrum of toxicities. *J Neurochem,* 150**,** 522-534.

ALVAREZ-ERVITI, L., RODRIGUEZ-OROZ, M. C., COOPER, J. M., CABALLERO, C., FERRER, I., OBESO, J. A. & SCHAPIRA, A. H. 2010. Chaperone-mediated autophagy markers in Parkinson disease brains. *Arch Neurol,* 67**,** 1464-72.

ANDERSON, J. P., WALKER, D. E., GOLDSTEIN, J. M., DE LAAT, R., BANDUCCI, K., CACCAVELLO, R. J., BARBOUR, R., HUANG, J., KLING, K., LEE, M., DIEP, L., KEIM, P. S., SHEN, X., CHATAWAY, T., SCHLOSSMACHER, M. G., SEUBERT, P., SCHENK, D., SINHA, S., GAI, W. P. & CHILCOTE, T. J. 2006. Phosphorylation of Ser-129 is the dominant pathological modification of alpha-synuclein in familial and sporadic Lewy body disease. *J Biol Chem,* 281**,** 29739-52.

ARAWAKA, S., SATO, H., SASAKI, A., KOYAMA, S. & KATO, T. 2017. Mechanisms underlying extensive Ser129-phosphorylation in alpha-synuclein aggregates. *Acta Neuropathol Commun,* 5**,** 48.

BETEMPS, D., VERCHERE, J., BROT, S., MORIGNAT, E., BOUSSET, L., GAILLARD, D., LAKHDAR, L., MELKI, R. & BARON, T. 2014. Alpha-synuclein spreading in M83 mice brain revealed by detection of pathological alpha-synuclein by enhanced ELISA. *Acta Neuropathol Commun,* 2**,** 29.

BOUSSET, L., PIERI, L., RUIZ-ARLANDIS, G., GATH, J., JENSEN, P. H., HABENSTEIN, B., MADIONA, K., OLIERIC, V., BOCKMANN, A., MEIER, B. H. & MELKI, R. 2013. Structural and functional characterization of two alpha-synuclein strains. *Nat Commun,* 4**,** 2575.

BOVE, J., MARTINEZ-VICENTE, M. & VILA, M. 2011. Fighting neurodegeneration with rapamycin: mechanistic insights. *Nat Rev Neurosci,* 12**,** 437-52.

CHAU, K. Y., CHING, H. L., SCHAPIRA, A. H. & COOPER, J. M. 2009. Relationship between alpha synuclein phosphorylation, proteasomal inhibition and cell death: relevance to Parkinson's disease pathogenesis. *J Neurochem,* 110**,** 1005-13.

CUERVO, A. M., STEFANIS, L., FREDENBURG, R., LANSBURY, P. T. & SULZER, D. 2004. Impaired degradation of mutant alpha-synuclein by chaperone-mediated autophagy. *Science,* 305**,** 1292-5.

DAHMENE, M., BERARD, M. & OUESLATI, A. 2017. Dissecting the Molecular Pathway Involved in PLK2 Kinase-mediated alpha-Synuclein-selective Autophagic Degradation. *J Biol Chem,* 292**,** 3919-3928.

EMMANOUILIDOU, E., STEFANIS, L. & VEKRELLIS, K. 2010. Cell-produced alpha-synuclein oligomers are targeted to, and impair, the 26S proteasome. *Neurobiol Aging,* 31**,** 953-68.

FLAVIN, W. P., BOUSSET, L., GREEN, Z. C., CHU, Y., SKARPATHIOTIS, S., CHANEY, M. J., KORDOWER, J. H., MELKI, R. & CAMPBELL, E. M. 2017. Endocytic vesicle rupture is a conserved mechanism of cellular invasion by amyloid proteins. *Acta Neuropathol,* 134**,** 629-653.

FUJIWARA, H., HASEGAWA, M., DOHMAE, N., KAWASHIMA, A., MASLIAH, E., GOLDBERG, M. S., SHEN, J., TAKIO, K. & IWATSUBO, T. 2002. alpha-Synuclein is phosphorylated in synucleinopathy lesions. *Nat Cell Biol,* 4**,** 160-4.

GAO, J., PERERA, G., BHADBHADE, M., HALLIDAY, G. M. & DZAMKO, N. 2019. Autophagy activation promotes clearance of alpha-synuclein inclusions in fibril-seeded human neural cells. *J Biol Chem,* 294**,** 14241-14256.

GOEDERT, M., JAKES, R. & SPILLANTINI, M. G. 2017. The Synucleinopathies: Twenty Years On. *J Parkinsons Dis,* 7**,** S51-S69.

GRASSI, D., DIAZ-PEREZ, N., VOLPICELLI-DALEY, L. A. & LASMEZAS, C. I. 2019. Palpha-syn* mitotoxicity is linked to MAPK activation and involves tau phosphorylation and aggregation at the mitochondria. *Neurobiol Dis,* 124**,** 248-262.

GRIBAUDO, S., TIXADOR, P., BOUSSET, L., FENYI, A., LINO, P., MELKI, R., PEYRIN, J. M. & PERRIER, A. L. 2019. Propagation of alpha-Synuclein Strains within Human Reconstructed Neuronal Network. *Stem Cell Reports,* 12**,** 230-244.

KARAMPETSOU, M., ARDAH, M. T., SEMITEKOLOU, M., POLISSIDIS, A., SAMIOTAKI, M., KALOMOIRI, M., MAJBOUR, N., XANTHOU, G., EL-AGNAF, O. M. A. & VEKRELLIS, K. 2017. Phosphorylated exogenous alpha-synuclein fibrils exacerbate pathology and induce neuronal dysfunction in mice. *Sci Rep,* 7**,** 16533.

KARPOWICZ, R. J., JR., HANEY, C. M., MIHAILA, T. S., SANDLER, R. M., PETERSSON, E. J. & LEE, V. M. 2017. Selective imaging of internalized proteopathic alpha-synuclein seeds in primary neurons reveals mechanistic insight into transmission of synucleinopathies. *J Biol Chem,* 292**,** 13482-13497.

LINDERSSON, E., BEEDHOLM, R., HOJRUP, P., MOOS, T., GAI, W., HENDIL, K. B. & JENSEN, P. H. 2004. Proteasomal inhibition by alpha-synuclein filaments and oligomers. *J Biol Chem,* 279**,** 12924-34.

LUK, K. C., KEHM, V., CARROLL, J., ZHANG, B., O'BRIEN, P., TROJANOWSKI, J. Q. & LEE, V. M. 2012. Pathological alpha-synuclein transmission initiates Parkinson-like neurodegeneration in nontransgenic mice. *Science,* 338**,** 949-53.

LUK, K. C., SONG, C., O'BRIEN, P., STIEBER, A., BRANCH, J. R., BRUNDEN, K. R., TROJANOWSKI, J. Q. & LEE, V. M. 2009. Exogenous alpha-synuclein fibrils seed the formation of Lewy body-like intracellular inclusions in cultured cells. *Proc Natl Acad Sci U S A,* 106**,** 20051-6.

MACHIYA, Y., HARA, S., ARAWAKA, S., FUKUSHIMA, S., SATO, H., SAKAMOTO, M., KOYAMA, S. & KATO, T. 2010. Phosphorylated alpha-synuclein at Ser-129 is targeted to the proteasome pathway in a ubiquitin-independent manner. *J Biol Chem,* 285**,** 40732-44.

MANECKA, D. L., VANDERPERRE, B., FON, E. A. & DURCAN, T. M. 2017. The Neuroprotective Role of Protein Quality Control in Halting the Development of Alpha-Synuclein Pathology. *Front Mol Neurosci,* 10**,** 311.

MASUDA-SUZUKAKE, M., NONAKA, T., HOSOKAWA, M., OIKAWA, T., ARAI, T., AKIYAMA, H., MANN, D. M. & HASEGAWA, M. 2013. Prion-like spreading of pathological alpha-synuclein in brain. *Brain,* 136**,** 1128-38.

MAZZULLI, J. R., ZUNKE, F., ISACSON, O., STUDER, L. & KRAINC, D. 2016. alpha-Synuclein-induced lysosomal dysfunction occurs through disruptions in protein trafficking in human midbrain synucleinopathy models. *Proc Natl Acad Sci U S A,* 113**,** 1931-6.

MELKI, R. 2015. Role of Different Alpha-Synuclein Strains in Synucleinopathies, Similarities with other Neurodegenerative Diseases. *J Parkinsons Dis,* 5**,** 217-27.

MORI, F., TANJI, K., YOSHIMOTO, M., TAKAHASHI, H. & WAKABAYASHI, K. 2002. Demonstration of alpha-synuclein immunoreactivity in neuronal and glial cytoplasm in normal human brain tissue using proteinase K and formic acid pretreatment. *Exp Neurol,* 176**,** 98-104.

MOUGENOT, A. L., NICOT, S., BENCSIK, A., MORIGNAT, E., VERCHERE, J., LAKHDAR, L., LEGASTELOIS, S. & BARON, T. 2012. Prion-like acceleration of a synucleinopathy in a transgenic mouse model. *Neurobiol Aging,* 33**,** 2225-8.

NEUMANN, M., MULLER, V., KRETZSCHMAR, H. A., HAASS, C. & KAHLE, P. J. 2004. Regional distribution of proteinase K-resistant alpha-synuclein correlates with Lewy body disease stage. *J Neuropathol Exp Neurol,* 63**,** 1225-35.

OUESLATI, A. 2016. Implication of Alpha-Synuclein Phosphorylation at S129 in Synucleinopathies: What Have We Learned in the Last Decade? *J Parkinsons Dis,* 6**,** 39-51.

OUESLATI, A., SCHNEIDER, B. L., AEBISCHER, P. & LASHUEL, H. A. 2013. Polo-like kinase 2 regulates selective autophagic alpha-synuclein clearance and suppresses its toxicity in vivo. *Proc Natl Acad Sci U S A,* 110**,** E3945-54.

PEELAERTS, W., BOUSSET, L., VAN DER PERREN, A., MOSKALYUK, A., PULIZZI, R., GIUGLIANO, M., VAN DEN HAUTE, C., MELKI, R. & BAEKELANDT, V. 2015. alpha-Synuclein strains cause distinct synucleinopathies after local and systemic administration. *Nature,* 522**,** 340-4.

PENG, C., GATHAGAN, R. J., COVELL, D. J., MEDELLIN, C., STIEBER, A., ROBINSON, J. L., ZHANG, B., PITKIN, R. M., OLUFEMI, M. F., LUK, K. C., TROJANOWSKI, J. Q. & LEE, V. M. 2018. Cellular milieu imparts distinct pathological alpha-synuclein strains in alpha-synucleinopathies. *Nature,* 557**,** 558-563.

PIERI, L., MADIONA, K. & MELKI, R. 2016. Structural and functional properties of prefibrillar alpha-synuclein oligomers. *Sci Rep,* 6**,** 24526.

SACINO, A. N., BROOKS, M., MCGARVEY, N. H., MCKINNEY, A. B., THOMAS, M. A., LEVITES, Y., RAN, Y., GOLDE, T. E. & GIASSON, B. I. 2013. Induction of CNS alpha-synuclein pathology by fibrillar and non-amyloidogenic recombinant alpha-synuclein. *Acta Neuropathol Commun,* 1**,** 38.

SACINO, A. N., BROOKS, M., MCKINNEY, A. B., THOMAS, M. A., SHAW, G., GOLDE, T. E. & GIASSON, B. I. 2014a. Brain injection of alpha-synuclein induces multiple proteinopathies, gliosis, and a neuronal injury marker. *J Neurosci,* 34**,** 12368-78.

SACINO, A. N., BROOKS, M., THOMAS, M. A., MCKINNEY, A. B., LEE, S., REGENHARDT, R. W., MCGARVEY, N. H., AYERS, J. I., NOTTERPEK, L., BORCHELT, D. R., GOLDE, T. E. & GIASSON, B. I. 2014b. Intramuscular injection of alpha-synuclein induces CNS alpha-synuclein pathology and a rapid-onset motor phenotype in transgenic mice. *Proc Natl Acad Sci U S A,* 111**,** 10732-7.

SACINO, A. N., BROOKS, M., THOMAS, M. A., MCKINNEY, A. B., MCGARVEY, N. H., RUTHERFORD, N. J., CEBALLOS-DIAZ, C., ROBERTSON, J., GOLDE, T. E. & GIASSON, B. I. 2014c. Amyloidogenic alpha-synuclein seeds do not invariably induce rapid, widespread pathology in mice. *Acta Neuropathol,* 127**,** 645-65.

712 SACINO, A. N., BROOKS, M. M., CHAKRABARTY, P., SAHA, K., KHOSHBOUEI, H.,
713 GOLDE, T. E. & GIASSON, B. I. 2017. Proteolysis of alpha-synuclein fibrils in
714 the lysosomal pathway limits induction of inclusion pathology. *J Neurochem,*
715 140**,** 662-678.
716 SHAHPASANDZADEH, H., POPOVA, B., KLEINKNECHT, A., FRASER, P. E., OUTEIRO, T. F.
717 & BRAUS, G. H. 2014. Interplay between sumoylation and phosphorylation
718 for protection against alpha-synuclein inclusions. *J Biol Chem,* 289**,** 31224-40.
719 STEFANIS, L., EMMANOUILIDOU, E., PANTAZOPOULOU, M., KIRIK, D., VEKRELLIS, K. &
720 TOFARIS, G. K. 2019. How is alpha-synuclein cleared from the cell? *J*
721 *Neurochem,* 150**,** 577-590.
722 TANIDA, I., UENO, T. & KOMINAMI, E. 2008. LC3 and Autophagy. *Methods Mol Biol,*
723 445**,** 77-88.
724 TANIK, S. A., SCHULTHEISS, C. E., VOLPICELLI-DALEY, L. A., BRUNDEN, K. R. & LEE, V.
725 M. 2013. Lewy body-like alpha-synuclein aggregates resist degradation and
726 impair macroautophagy. *J Biol Chem,* 288**,** 15194-210.
727 TANJI, K., MORI, F., MIMURA, J., ITOH, K., KAKITA, A., TAKAHASHI, H. &
728 WAKABAYASHI, K. 2010. Proteinase K-resistant alpha-synuclein is deposited
729 in presynapses in human Lewy body disease and A53T alpha-synuclein
730 transgenic mice. *Acta Neuropathol,* 120**,** 145-54.
731 TENREIRO, S., REIMAO-PINTO, M. M., ANTAS, P., RINO, J., WAWRZYCKA, D.,
732 MACEDO, D., ROSADO-RAMOS, R., AMEN, T., WAISS, M., MAGALHAES, F.,
733 GOMES, A., SANTOS, C. N., KAGANOVICH, D. & OUTEIRO, T. F. 2014.
734 Phosphorylation modulates clearance of alpha-synuclein inclusions in a yeast
735 model of Parkinson's disease. *PLoS Genet,* 10**,** e1004302.
736 UVERSKY, V. N. 2003. A protein-chameleon: conformational plasticity of alpha-
737 synuclein, a disordered protein involved in neurodegenerative disorders. *J*
738 *Biomol Struct Dyn,* 21**,** 211-34.
739 VEKRELLIS, K., XILOURI, M., EMMANOUILIDOU, E., RIDEOUT, H. J. & STEFANIS, L.
740 2011. Pathological roles of alpha-synuclein in neurological disorders. *Lancet*
741 *Neurol,* 10**,** 1015-25.
742 VEKRELLIS, K., XILOURI, M., EMMANOUILIDOU, E. & STEFANIS, L. 2009. Inducible
743 over-expression of wild type alpha-synuclein in human neuronal cells leads to
744 caspase-dependent non-apoptotic death. *J Neurochem,* 109**,** 1348-62.
745 VOGIATZI, T., XILOURI, M., VEKRELLIS, K. & STEFANIS, L. 2008. Wild type alpha-
746 synuclein is degraded by chaperone-mediated autophagy and
747 macroautophagy in neuronal cells. *J Biol Chem,* 283**,** 23542-56.
748 VOLPICELLI-DALEY, L. A., GAMBLE, K. L., SCHULTHEISS, C. E., RIDDLE, D. M., WEST, A.
749 B. & LEE, V. M. 2014. Formation of alpha-synuclein Lewy neurite-like
750 aggregates in axons impedes the transport of distinct endosomes. *Mol Biol*
751 *Cell,* 25**,** 4010-23.
752 VOLPICELLI-DALEY, L. A., LUK, K. C., PATEL, T. P., TANIK, S. A., RIDDLE, D. M., STIEBER,
753 A., MEANEY, D. F., TROJANOWSKI, J. Q. & LEE, V. M. 2011. Exogenous alpha-
754 synuclein fibrils induce Lewy body pathology leading to synaptic dysfunction
755 and neuron death. *Neuron,* 72**,** 57-71.
756 WAXMAN, E. A. & GIASSON, B. I. 2008. Specificity and regulation of casein kinase-
757 mediated phosphorylation of alpha-synuclein. *J Neuropathol Exp Neurol,* 67**,**
758 402-16.

759 WAXMAN, E. A. & GIASSON, B. I. 2010. A novel, high-efficiency cellular model of
760 fibrillar alpha-synuclein inclusions and the examination of mutations that
761 inhibit amyloid formation. *J Neurochem,* 113**,** 374-88.
762 WEBB, J. L., RAVIKUMAR, B., ATKINS, J., SKEPPER, J. N. & RUBINSZTEIN, D. C. 2003.
763 Alpha-Synuclein is degraded by both autophagy and the proteasome. *J Biol*
764 *Chem,* 278**,** 25009-13.
765 WINSLOW, A. R., CHEN, C. W., CORROCHANO, S., ACEVEDO-AROZENA, A., GORDON,
766 D. E., PEDEN, A. A., LICHTENBERG, M., MENZIES, F. M., RAVIKUMAR, B.,
767 IMARISIO, S., BROWN, S., O'KANE, C. J. & RUBINSZTEIN, D. C. 2010. alpha-
768 Synuclein impairs macroautophagy: implications for Parkinson's disease. *J*
769 *Cell Biol,* 190**,** 1023-37.
770
771
772

Figures and Legends

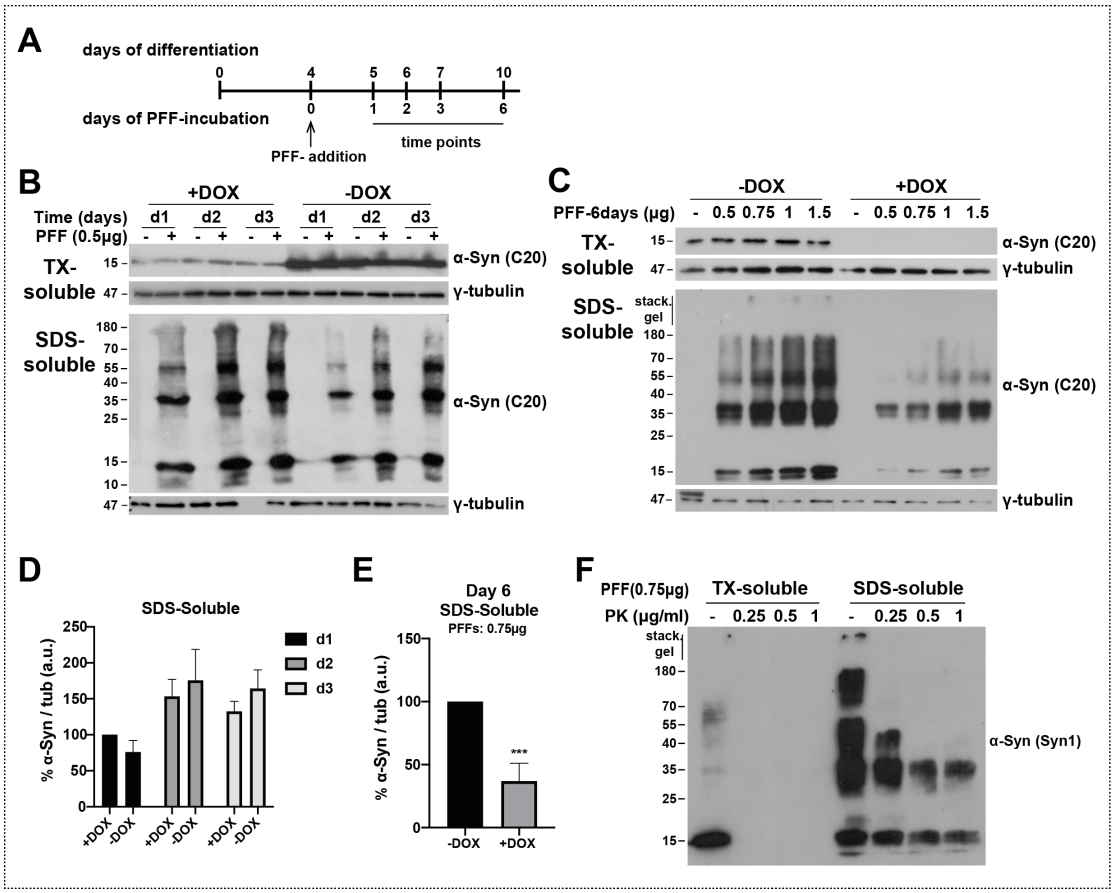

Figure 1. Time-dependence of seeding and aggregation of endogenous *α*-Syn in SH-SY5Y differentiated cells upon exposure to PFFs. A. SH-SY5Y cells, with inducible *α*-Syn overexpression (tet-off system), were differentiated for 4 days with RA (10µM) in the presence (+) or absence (-) of DOX. In -and +DOX cells, PFFs were added and *α*-Syn aggregation was assessed 1, 2, 3 and 6 days post-PFF addition. **B.** 1, 2 and 3 days after PFF-addition (0.5µg), cells were harvested and subjected to fractionation, followed by western immunoblotting (TX-100 and SDS fraction) with an antibody against total *α*-Syn (C20). **C.** After 6 days of PFF-incubation, using different amounts of PFFs (0, 0.5, 0.75, 1, 1.5 µg), cells were harvested and subjected to fractionated western immunoblotting with an antibody against total *α*-Syn (C20). γ-tubulin was used as a loading control. **D, E.** Quantification of SDS-soluble *α*-Syn levels (monomeric and HMW species) in - and + Dox cells after 1, 2, 3 (**D**) and 6 days (**E**) of PFF-incubation. Data is presented as the mean ± SE of 3 (**D**) and 4 (**E**) independent cell culture preparations; one-way ANOVA with Bonferonni's correction was used for (**D**) and Student's t-test for (**E**). Statistical significance was set as *** p<0.001. **F.** Cells were harvested 6 days post-PFF, fractionated and subjected to Proteinase K (PK) treatment, followed by western immunoblotting with an antibody against total *α*-Syn (Syn1).

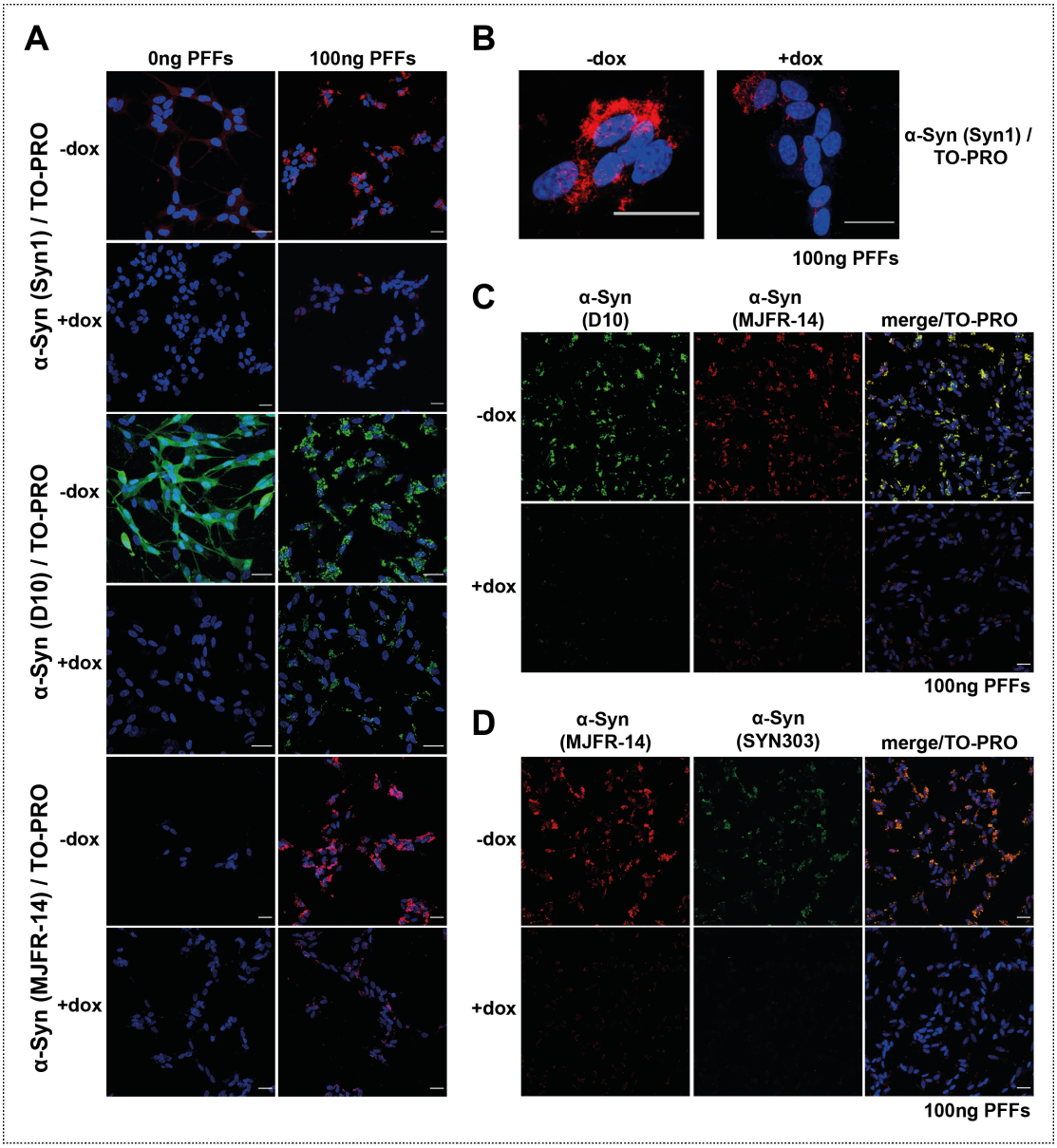

Figure 2. Accumulation of endogenous α-Syn aggregates 6 days after PFF addition. A. Differentiated SH-SY5Y cells, -Dox and +Dox, were incubated with PFFs (100 ng) for 6 days, were fixed and immunostained with Syn1, D10, both detecting total α-Syn, and MJFR-14, detecting aggregated α-Syn species. Representative confocal images depict α-Syn aggregates in -Dox cells. **B.** Higher magnification confocal images show α-Syn aggregates detected around the nucleus in -Dox cells. **C.** Double labelling immunofluorescent analysis of differentiated SH-SY5Y cells using total α-Syn antibody, D10, in conjunction with MJFR-14, detecting aggregated α-Syn. **D.** Immunofluorescent images of differentiated SH-SY5Y cells double labelled with antibodies detecting aggregated α-Syn (MJFR-14) and oxidized/nitrated α-Syn (SYN303). TO-PRO was used to stain the nucleus. Expression of α-Syn was observed using fluorescence confocal microscopy. Scale bar 30 µm.

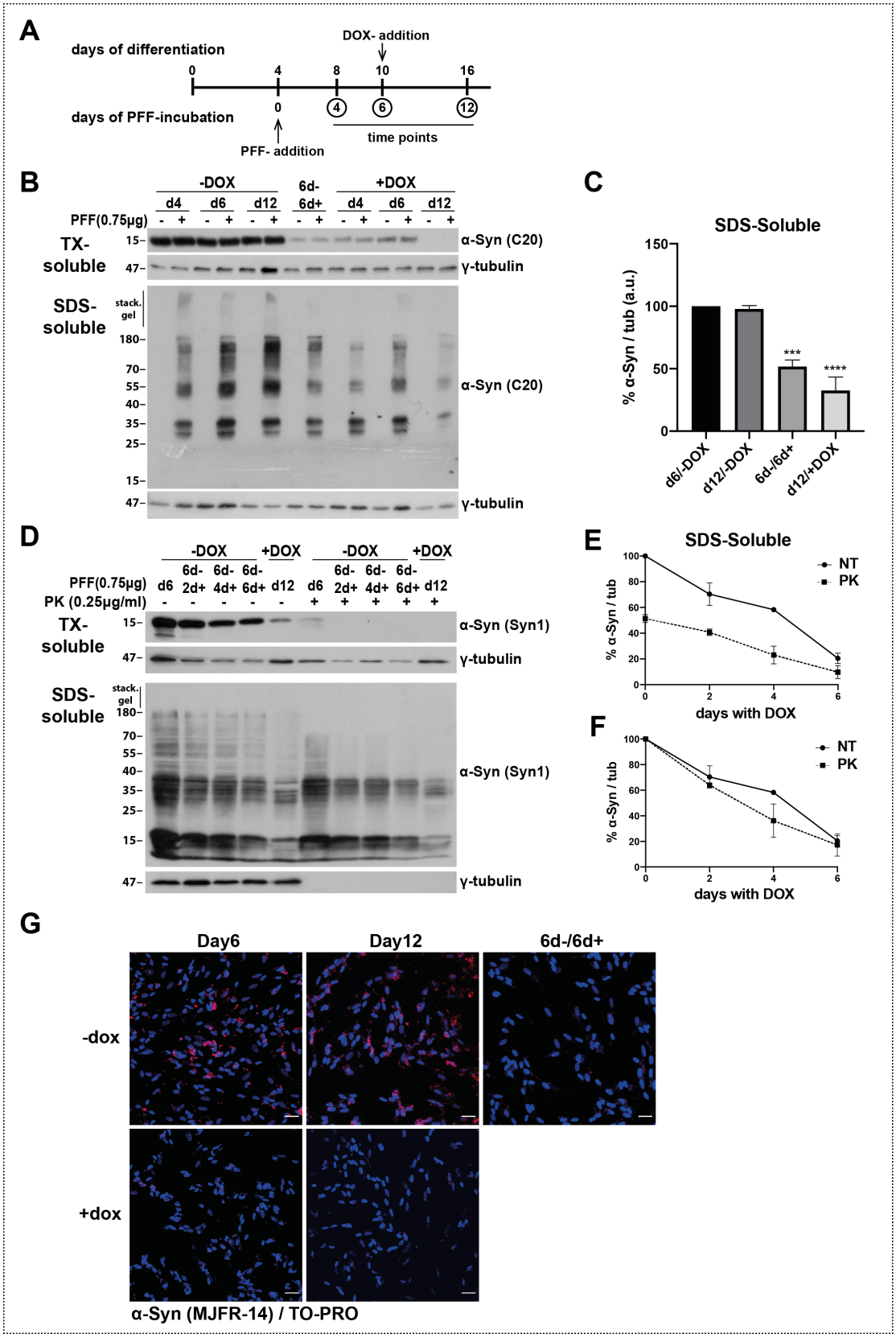

Figure 3. Seeding and degradation of endogenous *α*-Syn in SH-SY5Y differentiated cells upon PFF-incubation is more prominent over time, and seeded *α*-Syn is cleared from the cells upon shutdown of *α*-Syn expression. A. In differentiated - and +DOX cells, PFFs were added and the cells were incubated for 6 and 12 days. Cells overexpressing *α*-Syn (-DOX)

were incubated 6 days with PFFs, and then with DOX for the following 6 days in order to suppress α-Syn expression (6d-/6d+). **B.** After 4, 6 and 12 days of PFF-incubation (0,75μg), cells were harvested and subjected to fractionation and western immunoblotting (TX-100 and SDS fraction) with an antibody against α-Syn (C20). **C.** Quantification of SDS-soluble α-Syn levels in - and + Dox, and in 6d-/6d+ cells after 6 and 12 days of PFF-addition from 5 independent cell culture preparations. One-way ANOVA with Bonferonni's correction was used. **D.** Cells overexpressing α-Syn (-DOX) were incubated 6 days with PFFs, and then with DOX for the following 2 (6d-/2d+), 4 (6d-/4d+) and 6 (6d-/6d+) days. +DOX cells, after 12 days of PFF-addition, were used as a control. Cells were harvested, fractionated and subjected to Proteisase K (PK) treatment, followed by western immunoblotting with an antibody against total α-Syn (Syn1). γ-tubulin was used as a loading control. **E, F.** Quantification of SDS-soluble α-Syn levels in d6, 6d-/2d+, 6d-/4d+, 6d-/6d+ cells relatively to d6 protein levels of PK non-treated samples (**E**) and clearance rate of non-treated or treated with PK samples (**F**). Data is presented as the mean ± SE of 3 independent cell culture preparations; one-way ANOVA with Bonferonni's correction was used. Statistical significance was set as * $p<0.05$, ** $p<0.01$, *** $p<0.001$. **G.** Differentiated SH-SY5Y cells, -Dox, +Dox and 6d-/6d+, after 6 and 12 days of PFF-addition, were fixed and immunostained with MJFR-14, detecting aggregated α-Syn species. TO-PRO was used to stain the nucleus. Representative confocal images depict α-Syn aggregates in -Dox cells. Scale bar 30 μm.

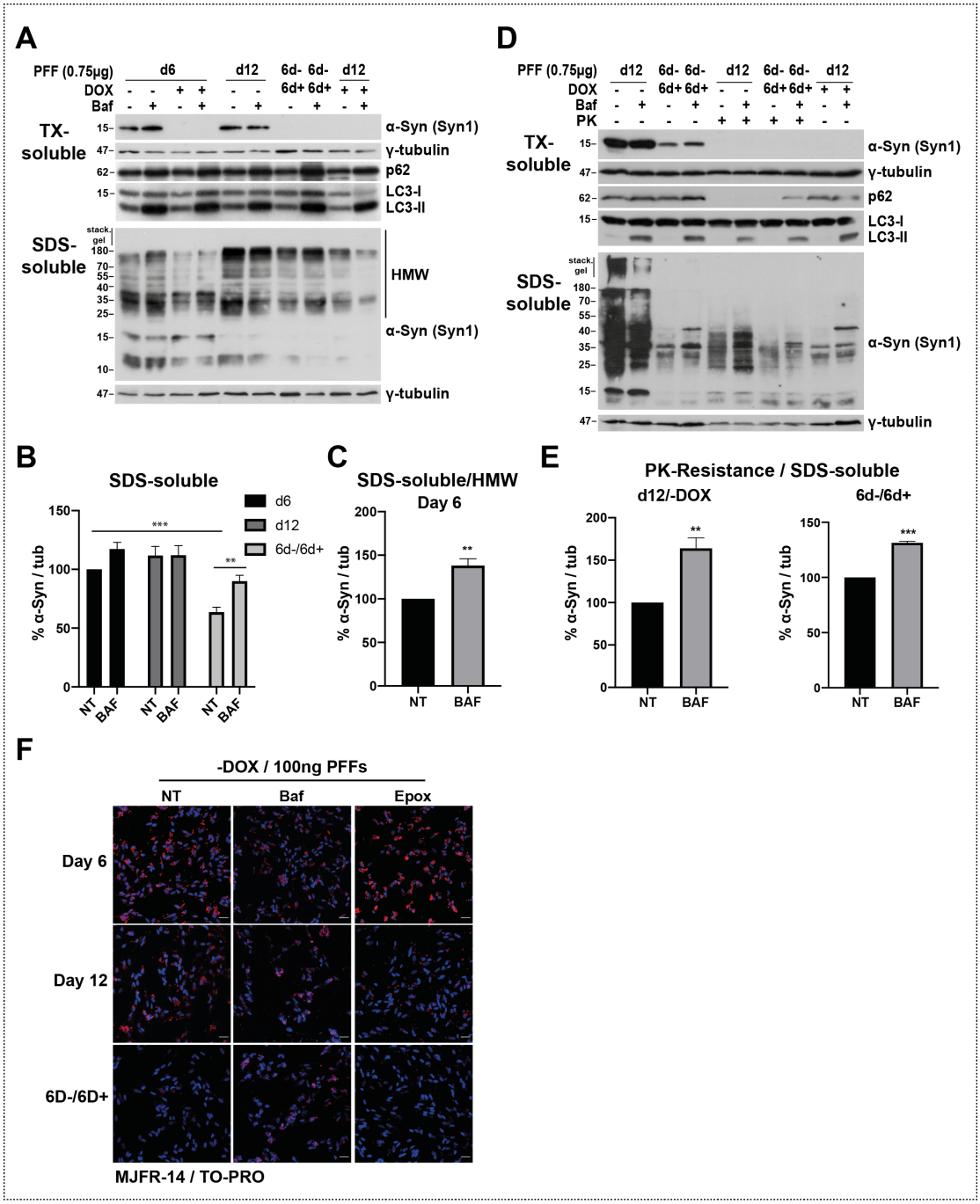

Figure 4. Clearance of seeded *α*-Syn is Lysosomal-dependent. A. In - and +DOX cells, PFFs were added and the cells were incubated for 6 and 12 days. Cells overexpressing *α*-Syn (-DOX) were incubated 6 days with PFFs, and then with DOX for the following 6 days in order to suppress *α*-Syn expression (6d-/6d+). 6 and 12 days after PFF-addition (0,75µg), non-treated and bafilomycin (Baf)- treated cells (100nM) were harvested and subjected to fractionated western immunoblotting (Tx-100 and SDS- soluble fraction) with an antibody against *α*-Syn (Syn1), p62 and LC3. γ-tubulin was used as a loading control. **B.** Quantification of SDS-soluble *α*-Syn levels in non-treated and bafilomycin-treated d6, d12 and 6d-/6d+ -DOX cells. **C.** Quantification of higher molecular weight (HMW) species of SDS-soluble *α*-Syn in non-treated and bafilomycin-treated d6 cells. **D.** 6 and 12 days after PFF-addition (0,75µg), non-treated and bafilomycin-treated cells (100nM) were harvested, fractionated

847 and subjected to PK treatment (0.25 μg/ml), followed by western immunoblotting (TX-100
848 and SDS fraction) with an antibody against *α*-Syn (Syn1), p62, LC3 and γ-tubulin. **E.**
849 Quantification of SDS-soluble *α*-Syn levels in non-treated and bafilomycin-treated d12 and
850 6d-/6d+ cells, treated with PK. For quantification (**B**, **E**) data is presented as the mean ± SE of
851 3 and for (**C**) from 5 independent cell culture preparations; two-way ANOVA with
852 Bonferonni's correction was used for (**B**) and student's t-test for (**C**, **E**). Statistical significance
853 was set as *p<0.05, **p<0.01, ***p<0.001. **F.** 6 and 12 days after PFF-addition (100ng), non-
854 treated and bafilomycin- or epoxomicin-treated -DOX, +DOX and 6d-/6d+ cells were fixed
855 and stained with anti-*α*-Syn (MJFR-14). TO-PRO was used to stain the nucleus. Expression of
856 aggregated *α*-Syn (MJFR-14) was observed using fluorescence confocal microscopy. Scale bar
857 30 μm.
858

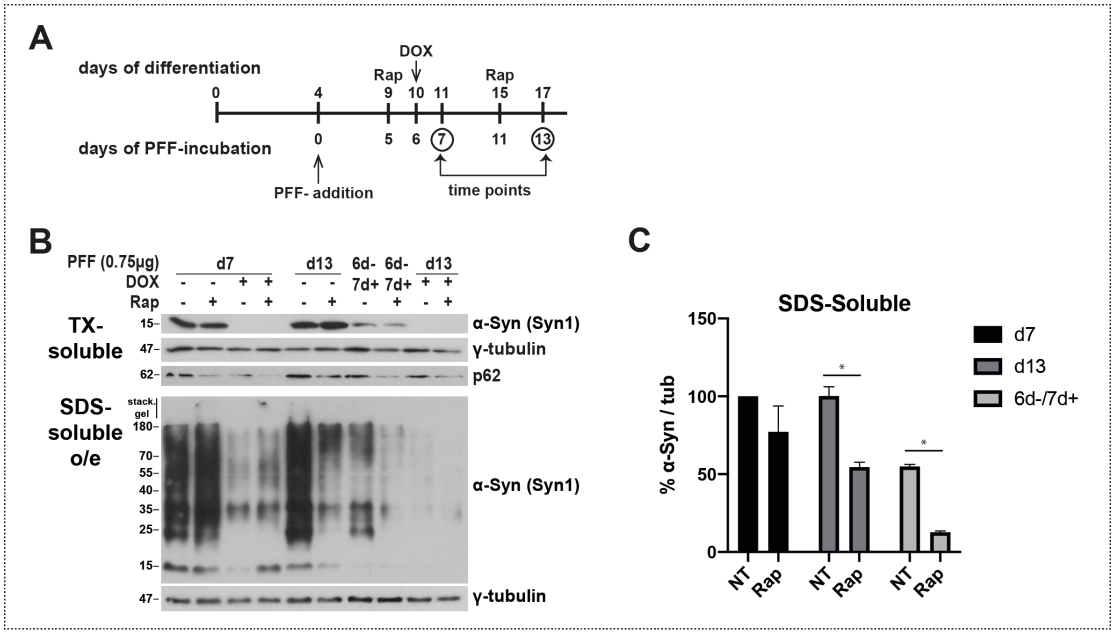

Figure 5. Rapamycin-mediated induction of Macroautophagy leads to the clearance of fibrillar *α*-Syn. A. In -DOX and +DOX differentiated cells, PFFs were added and aggregation was assessed 7 and 13 days post-PFF. 6 days post-PFF, -DOX cells were incubated with DOX for the following 7 days in order to suppress *α*-Syn expression (6d-/7d+). Rapamycin was added in the cultures 48h before harvesting the cells. **B.** Non-treated and rapamycin-treated cells (1µM) were harvested and subjected to fractionated western immunoblotting (TX-100 and SDS fraction) with an antibody against *α*-Syn (Syn1), p62 and γ-tubulin. **C.** Quantification of SDS-soluble *α*-Syn levels in non-treated and rapamycin-treated d7, d13 and 6d-/7d+ cells. Data is presented as the mean ± SE of 3 independent cell culture preparations; two-way ANOVA with Bonferonni's correction was used. Statistical significance was set as *p<0.05.

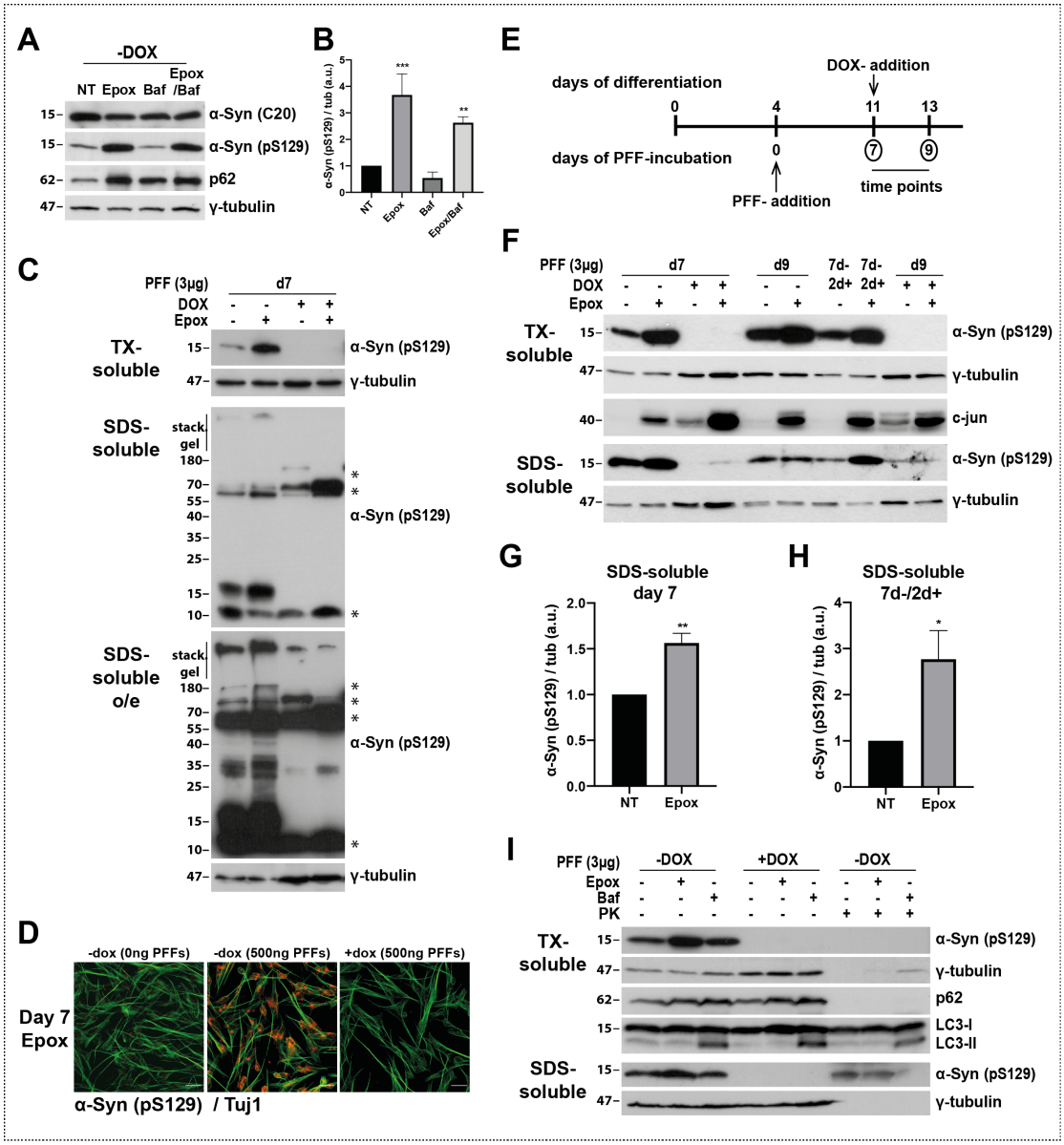

Figure 6. Proteasomal inhibition leads to accumulation of both TX- and SDS- soluble phosphorylated *α*-Syn. A. Differentianted SH-SY5Y cells overexpressing *α*-Syn (-DOX) were treated with epoxomicin (Epox), bafilomycin (Baf) or with both inhibitors (Epox/Baf) for 24h, harvested and lysed with 1% SDS RIPA Buffer. The lysates were subjected to western immunoblotting with anti-*α*-Syn (C20), anti-pS129, anti-p62, and anti-γ-tubulin antibodies. **B.** Quantification of phosphorylated *α*-Syn levels in epoxomicin-, bafilomycin- and epoxomicin/bafilomycin- treated cells. **C.** After 7 days of high-dose PFF (3 μg) incubation, -and +DOX cells, non-treated and epoxomicin-treated, were subjected to fractionated western immunoblotting (TX-100 and SDS fraction) with anti-pS129 and anti-γ-tubulin antibodies. Monomeric and higher molecular weight bands of pS129 *α*-Syn were detected (*: non-specific bands). **D**. After 7 days of PFF-incubation (500ng) and epoxomicin treatment (24h incubation before staining), differentiated SH-SY5Y cells were analyzed by immunocytochemistry with anti-*α*-Syn (pS129) and anti-Tuj1 antibodies. Expression of pS129 *α*-Syn (red) and Tuj1 (green) was observed using fluorescence confocal microscopy. Scale bar 30 μm. **E.** 7 and 9 days after high-dose PFF (3 μg) addition, differentiated SH-SY5Y cells (- or

+DOX and 7d-/2d+), untreated or treated with epoxomicin for 24 hours, were assessed for fibrillar pS129 α-Syn. **F.** Cells were harvested and subjected to fractionated western immunoblotting (Tx-100 and SDS soluble fraction) with anti-pS129, anti-cjun, and anti-γ-tubulin antibodies. **G, H.** Quantification of SDS-soluble phosphorylated α-Syn levels in d7 -DOX (**G**) and 7d-/2d+ (**H**) cells. For quantification (B, G and H), data is presented as the mean ± SE of 3 independent cell culture preparations; one-way ANOVA with Bonferonni's correction was used for (**B**) and student's t-test for (**G**) and (**H**). Statistical significance was set as *p<0.05, **p<0.01, ***p<0.001. **I.** 7 days after high-dose PFF (3 μg) addition, - and +DOX cells, non-treated, epoxomicin- or bafilomycin- treated, were lysed, fractionated and subjected to PK treatment, followed by western immunoblotting with anti-pS129, anti-p62, anti-LC3 and anti-γ-tubulin antibodies. Representative blot from 2 independent cell culture preparations.

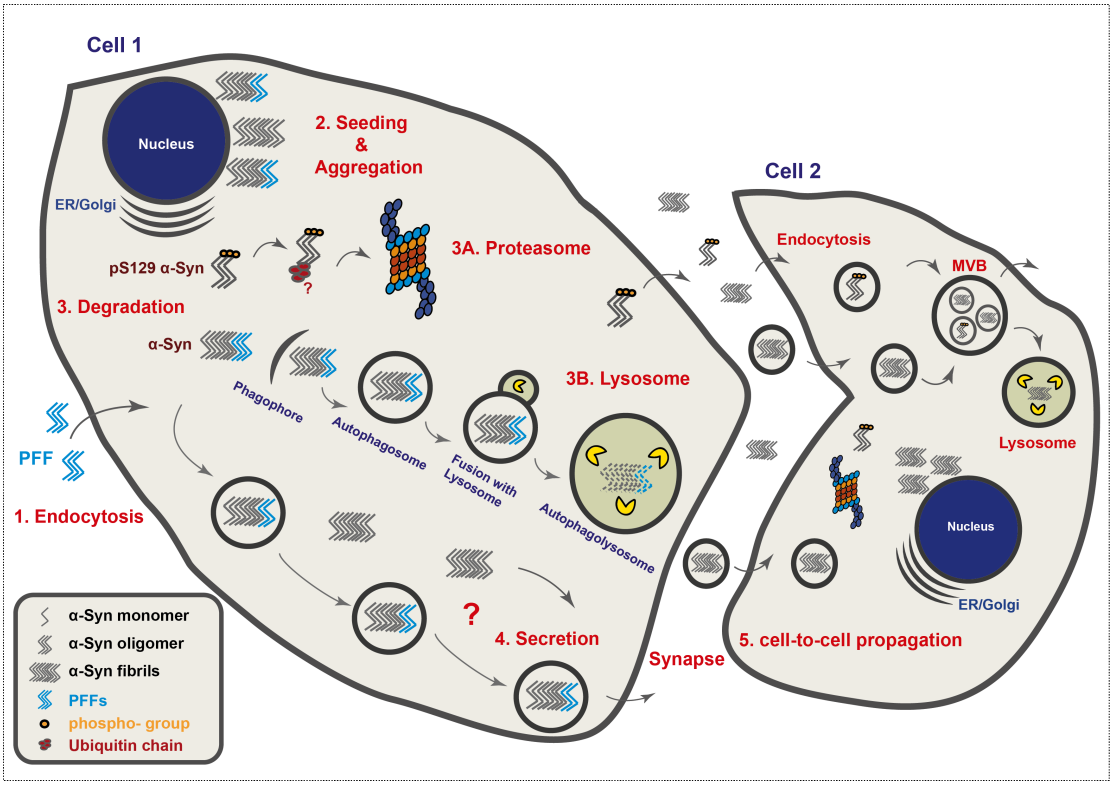

Figure 7. Schematic illustration of the SH-SY5Y inducible neuronal model, fine-tuned for investigating aggregated α-Syn turnover. SH-SY5Y differentiated cells with inducible expression of α-Syn can serve as a model to investigate aggregation propensity and clearance of PFF-triggered α-Syn assemblies. PFFs are internalized within 48h (**1**) and 6 days post-PFF, endogenous α-Syn is seeded and detected mostly around the nucleus (**2**). Downregulation of α-Syn upon doxycycline addition results in the clearance of α-Syn aggregates (**3**), however reversed when lysosomal inhibitors are used. Together with the rapamycin effect, autophagy (macro- or micro-) seems to serve as the major pathway for SDS-soluble α-Syn clearance (**3B**). Phosphorylated at S129 α-Syn aggregates, with limited PK resistance, are detected only when high-dose of PFFs are used. These assemblies accumulate further when the proteasome is inhibited, pointing out the role of the Ubiquitin

916 Proteasome System in the degradation of phosphorylated *α*-Syn aggregates (**3A**). *α*-Syn
917 aggregates could be further secreted (**4**) and uptaken by neighbouring cells (**5**). This fine-
918 tuned inducible neuronal model can be used to further investigate components of the
919 degradation pathways aggregated *α*-Syn follows as well as the mechanisms involved in *α*-Syn
920 secretion and cell-to-cell propagation.
921